

# From motor-induced fluctuations to mesoscopic dynamics in epithelial tissues

É. Fodor,<sup>1,\*</sup> V. Mehandia,<sup>2,3,\*</sup> J. Comelles,<sup>2</sup> R. Thiagarajan,<sup>2</sup> N. S. Gov,<sup>4</sup> P. Visco,<sup>1</sup> F. van Wijland,<sup>1</sup> and D. Riveline<sup>2</sup>

<sup>1</sup>*Laboratoire Matière et Systèmes Complexes, UMR 7057 CNRS/P7, Université Paris Diderot,  
10 rue Alice Domon et Léonie Duquet, 75205 Paris cedex 13, France*

<sup>2</sup>*Laboratory of Cell Physics, ISIS/IGBMC, Université de Strasbourg and CNRS (UMR 7006),  
8 allée Gaspard Monge, 67083 Strasbourg, France Development and Stem Cells Program,  
IGBMC, CNRS (UMR 7104), INSERM (U964), Université de Strasbourg,  
1 rue Laurent Fries, BP10142, 67400 Illkirch, France*

<sup>3</sup>*School of Mechanical, Materials and Energy Engineering, Indian Institute of Technology Ropar, India*

<sup>4</sup>*Department of Chemical Physics, Weizmann Institute of Science, 76100 Rehovot, Israel*

(Dated: December 7, 2015)

Molecular motors power spatial fluctuations in epithelial tissues. We evaluate these fluctuations in MDCK monolayers by tracking tricellular junctions, leading us to highlight the non-Gaussian statistics of the junction displacement. Using a mesoscopic framework which separates the thermal fluctuations originating from the heat bath and the athermal ones generated by the motors, we quantify key parameters of the junction activity such as diffusion coefficient, persistence time and persistence length. When inhibiting specific targets in the molecular pathway which regulates the motors, we report subsequent modifications of these parameters: the hierarchy in the molecular pathway is correlated to the active fluctuations driving the junction dynamics. Our study provides a framework for quantifying nonequilibrium fluctuations in living matter with potential relevance for physiological shape transformations in the developing embryos.

PACS numbers: 87.17.-d, 87.18.Tt, 87.18.Fx

Living and non-living matter show a variety of fluctuations at different length and timescales. Measuring these fluctuations is an effective way to study nonequilibrium systems. In living cells, it is the continuous supply of energy from the hydrolysis of ATP/GTP which takes the system out-of-equilibrium. New models are proposed to describe this nonequilibrium dynamics [1–9], yielding a proper definition of energy dissipation as related to spatial fluctuations [10–13]. One class of models exploits the similarities and differences between foams and living tissues, where cells form a connected network of straight edges and vertices [14–17]. In living tissues, the spontaneous rearrangements between vertices reveal the nonequilibrium nature of their dynamics. A paradigmatic type of rearrangement correspond to neighboring cell exchanges, known as T1 transition [16, 18]. It is a key mechanism which drives the dramatic morphogenesis rearrangements in organisms such as dorsal closure in developing embryo [18–21]. The molecular origin of such transitions is associated with acto-myosin molecular motors [22, 23]. Yet, quantitative studies are lacking to understand the regulation of the tissue dynamics by these motors. It is our aim in this paper to investigate the mechanism driving the spatial fluctuations, using specific inhibition of the molecular pathway.

We explore the nonequilibrium active properties of epithelial monolayers by directly accessing the fluctuations of vertices. We first report the experimental methods and extraction of the data. We then present a model for the vertex dynamics, on the basis of which we characterize the vertex fluctuations in terms of time, length, and energy scales. Eventually, we highlight the biological significance of our results: the hierarchy in the molecular pathway regulating

the acto-myosin motors directly controls the active fluctuations of the vertices.

*Vertex tracking and inhibitors.*—We use Madin-Darby Canine Kidney (MDCK) cells stably transfected with E-cadherin fused with the Green Fluorescent Protein (GFP) as a paradigm for epithelial tissues dynamics [24]. This allows us to study live cells while interacting with each other. We seek to identify spatial points primarily involved in tissue transformations. The meeting points between three cells are involved in the exchanges between neighbouring cells, thus serving as hallmark of the tissue dynamics. We extract the vertex trajectories by tracking them as long as they are visible and in the absence of neighboring cell division, until a maximum of 8 hours [Fig. 1]. Namely, we do not follow the long time motion driven by cell division [25].

The vertex dynamics is driven by both thermal fluctuations produced by the heat bath, and the active fluctuations powered by the acto-myosin molecular motors. The myosin-II motors are localized in dense contractile units present in the apical surface of the tissue [22, 26], as shown in Figs. 1(a-c). Specifically, the Rho signalling pathway controls the acto-myosin activity in a specific manner inside cells (see Fig. 9 in [27]). Upstream and downstream targets install a hierarchy in the activation of myosin. To assess the relevance of the various ingredients of this pathway, we specifically inhibit different targets: Rho, Rho kinase (ROCK) and myosin-II [Fig. 1(f)]. We also investigate the roles of microtubules (MTs) by promoting their depolymerization, and we consider untreated cells as a control [28]. Altogether, we probe five conditions on the same system.

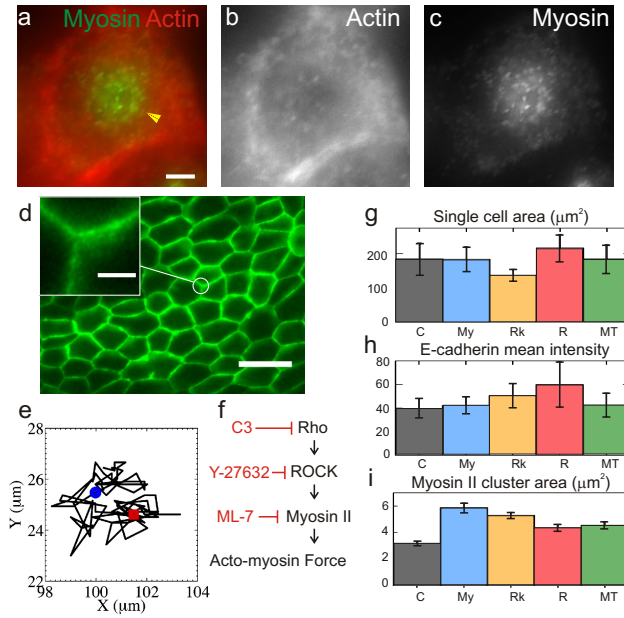


FIG. 1. (Color online) Study of the vertex fluctuations. (a) Actin (red) and myosin (green) structures at the apical surface of a MDCK cell (scale bar  $3 \mu\text{m}$ ). The myosin is concentrated in dense contractile units (yellow arrow) referred to as myosin clusters. (b) Actin structure alone. (c) Myosin structure alone. (d) We visualise MDCK cell monolayer by GFP E-cadherin (scale bar  $30 \mu\text{m}$ ). (inset) We identify the meeting points between three cells as the privileged point for our analysis. (scale bar  $4 \mu\text{m}$ ). (e) Extraction of a typical vertex trajectory of 8 hours beginning at the blue circle and ending at the red square with 5 minutes between each point. (f) Simplified diagram of the Rho pathway installing a hierarchy in acto-myosin activation; in red the specific inhibitors and their targets. (g) Area of individual cells in each condition. (h) Mean GFP E-cadherin intensity of individual cell-cell contacts. (i) Area of myosin clusters.

We investigate the effect of the different inhibitors on both the architecture and the contractile forces of the tissue by measuring single cell area, E-cadherin intensity and myosin cluster area in each condition. Single cell area is not strongly affected by the inhibitors, except for a reduced value in the Rho kinase inhibitor case, showing that the tissue architecture is barely affected by external inhibitors [Fig. 1(g)]. This is also true for the polygonicity distribution [28]. For what concerns E-cadherin intensity, we observe an increase, thus supporting that cell-cell adhesion is enhanced, upstream of the Rho pathway [Fig. 1(h)]. The MT depolymerization does not affect the E-cadherin intensity with respect to the control.

The mean density value of myosin clusters for control is larger than in the inhibited cases (see Fig. S2(b) in [28]), suggesting a decrease in force generation for the same level of myosin per cell. In addition, the area of each myosin cluster is smaller in control than in other conditions [Fig. 1(i)]. Besides, this area decreases upstream the

Rho pathway, suggesting a relaxation of the pool of myosin in the apical side, consistently with the notion that myosin force is reduced upstream the Rho pathway. Overall, we deduce that the myosin activity is decreased upstream the Rho pathway.

Because of the complexity of the processes driving the tissue dynamics, anticipating the response in the vertex fluctuations to the different inhibitors is largely a challenge to physical interpretation. Our goal is to propose a synthetic read-out to understand how the hierarchy in the Rho pathway is transferred to the cell-cell junction dynamics. To this aim, we study the statistics of the vertex fluctuations extracted from the individual trajectories.

*Statistics of the vertex fluctuations.*—First, we compute the projected one-dimensional mean square displacement (MSD) within the five different conditions [Fig. 2(a)]. For each condition, the power law behavior of the short time MSD shows an exponent close to 0.7. The large time MSD is more sensitive to the cell condition. The corresponding exponent is larger than 1, except for MT depolymerization where it is close to 1, and myosin inhibitor where it is smaller. The crossover between the two regimes appears between 20 and 60 min. The fluctuations are reduced in the myosin inhibited case, which has the lowest MSD, and they are enhanced for the Rho inhibitor, where the large time growth is the largest.

In addition, we explore the full statistics of vertex displacement by measuring the probability distribution function (PDF) for each condition, as shown in Figs. 2(b-f). At short time the PDF is Gaussian, while it exhibits broader tails at large time. As equilibrium fluctuations are usually associated with Gaussian statistics, we interpret the non-Gaussian tails as a signature of nonequilibrium fluctuations, driven by the cellular activity. These tails reveal large displacements of the vertex, and were already observed for tracer particles in active gels [29] and living cells [3, 30, 31]. They are more pronounced in Rho inhibitor and MT depolymerization cases, as a signature of larger fluctuations possibly due to directed motion events.

*Caging model.*—To quantitatively discriminate between the different conditions, we test our measurements with a nonequilibrium model, previously introduced in [3] to describe tracer fluctuations inside living cells. We regard the vertex as a virtual particle which dynamics is prescribed by two coupled equations: (i) an equilibrium diffusion of the vertex in a cage, modelled as a harmonic potential of stiffness  $k$ —the displacement is driven by a Gaussian white noise of variance  $2\gamma k_B T$  with a drag force of coefficient  $\gamma$ ; (ii) a non-Gaussian coloured diffusion equation for the center of the cage, mimicking nonequilibrium activity [28]. Inspired by the large ballistic-like displacements that we observe in experimental trajectories, we model this active noise as a two-state Poisson process: the cage has a constant velocity  $v$  in a random uniformly sampled two-dimensional direction during a random persistence time of average  $\tau$ , and it remains fixed during a random quiescence

time of mean  $\tau_0$ .

We understand the confinement as an elastic mechanical stress resulting from the cells surrounding each vertex, and the nonequilibrium motion of the cage as an active stress. The effect of this active stress is to reorganize the structure of the monolayer, and therefore to spatially redistribute the elastic mechanical stress. It is worth noting that this model would be compatible with considering that each cell junction acts as a spring on the vertex [32, 33]. By adding an active stress to these junctions, one would get a similar behavior for the vertex dynamics [28].

In the absence of activity, this model predicts a short time diffusion, and then a large time plateau expressing the elastic confinement [28]. Such dynamics is entirely under the control of equilibrium thermal fluctuations. In an active system, nonequilibrium processes enhance the vertex displacement *via* the cage motion, yielding a free diffusion of the vertex with coefficient  $D_A = (v\tau)^2/[2(\tau + \tau_0)]$ . The large time dynamics is fully determined by the active parameters  $\{v, \tau, \tau_0\}$ , whereas thermal fluctuations control the short times *via*  $\{k, \gamma, T\}$ . A sub-diffusive transient regime appears between the two diffusions, as a crossover towards a plateau, and a super-diffusive regime can also precede the large time diffusion, as a signature of the ballistic motion involved in the active noise. In such a case, thermal effects are negligible at times larger than  $\tau_s = \sqrt{\tau k_B T / (k D_A)}$ . This timescale quantifies the transition from the short time equilibrium-like dynamics to the large time active diffusion. When overlayed, simulated trajectories exhibit clusters of similar size accounting for the transient confinement of the vertex. Occasionally large displacements of order  $v\tau$  appear. The vertices do not only fluctuate around a local equilibrium position, they also undergo rapid directed jumps [Fig. 3(a)].

**Active diffusion coefficient and persistence length.**—We fit the MSD data to estimate the parameters characterizing nonequilibrium activity by using our analytic prediction [28]. Our fits convincingly capture the transient sub-diffusive and super-diffusive regimes [Fig. 2(a)]. We report clear quantitative variations of both the active diffusion coefficient  $D_A$  and the persistence length  $\tau$  between the five conditions. It establishes that our model, based on separating the purely active fluctuations from the equilibrium thermal ones, is a reliable framework to capture the effects of the molecular inhibitors on the tissue dynamics. In that respect,  $D_A$  and  $\tau$  are relevant parameters to characterize the vertex fluctuations. Therefore, our analysis indeed enables one to identify the role of each regulatory stage at a mesoscopic level.

Strikingly,  $D_A$  and  $\tau$  are larger for Rho inhibitor than for Rho kinase inhibitor, and than for direct myosin inhibition [Figs. 3(b,c)]. This demonstrates that the active fluctuations driving the vertex dynamics are under the control of the Rho pathway: the more upstream in the pathway, the larger the amplitude of the fluctuations and the more persistent the ensuing displacement. In contrast, MT de-

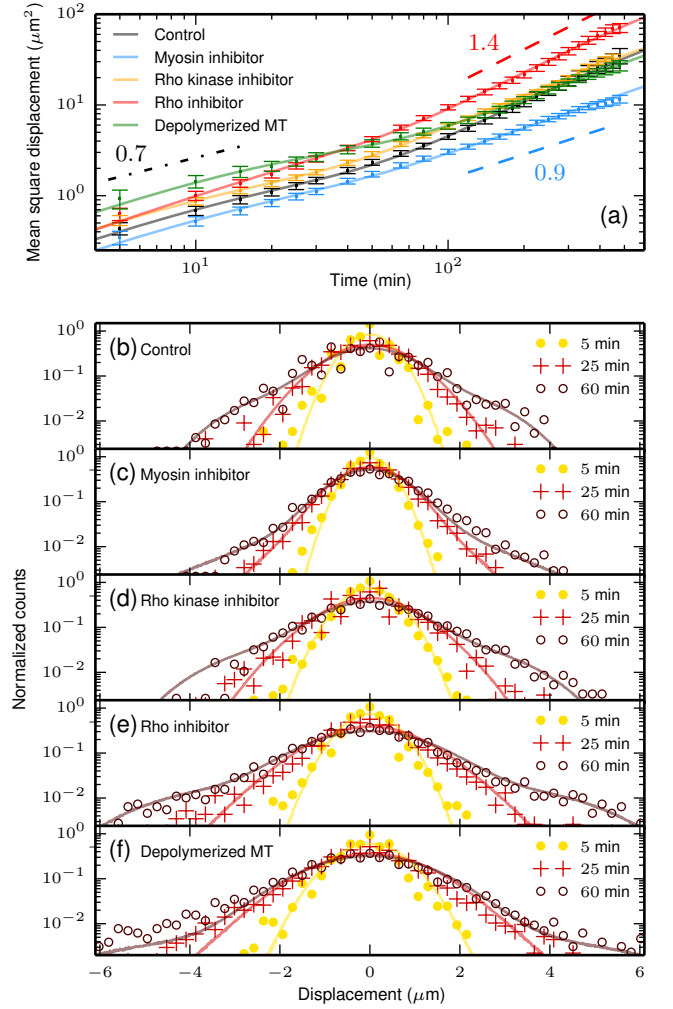


FIG. 2. (Color online) Statistics of the vertex fluctuations. (a) Mean square displacement as a function of time in five conditions: control (black), myosin inhibitor (blue), Rho kinase inhibitor (orange), Rho inhibitor (red), and microtubule depolymerization (green). The corresponding best fitting curves are in solid lines (Eq. (S5) [28]). The dot dashed line indicates the short time power law, whereas the blue and red dashed lines report the large time behaviors. (b-f) Distribution of displacement for the five conditions at three times: 5 min (●), 25 min (+), and 60 min (○). Exponential tails appear at long times as a consequence of directed motion events in the vertex dynamics. Results of the simulated dynamics are in solid lines.

polymerization does not result in major changes in the extracted parameters with respect to the control condition. It suggests that MTs do not affect the vertex dynamics *per se*. This may be supported by the essential role of MTs in material transport, consistently with functions already reported for focal contact dynamics [34]. Eventually, our estimation of  $\tau_s$  is to be compared with timescales quantifying the transition from elastic to fluid-like behavior of the material [Fig. 3(c)]. In that respect, it is of the same order as the Maxwell time reported in three-dimensional cell



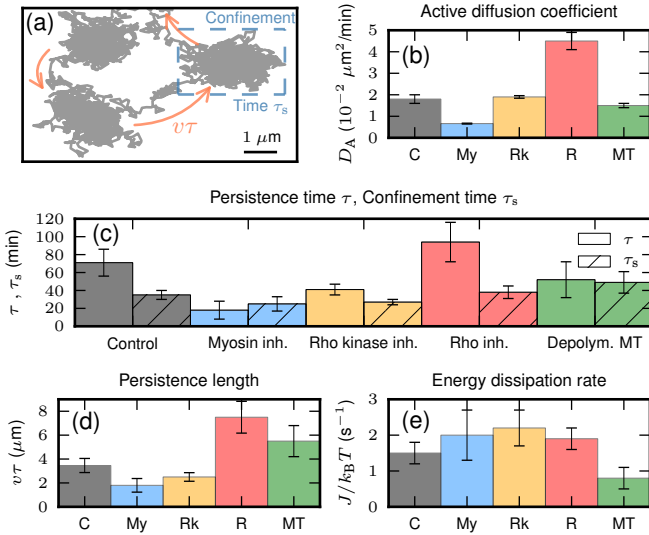


FIG. 3. (Color online) Active parameters of the vertex fluctuations. (a) Typical trajectory obtained from simulations of the vertex dynamics in control condition (scale bar 1  $\mu\text{m}$ ) [28]. Isotropic bundles reveal equilibrium-like transient confinement during a typical time  $\tau_s$  (dashed blue box), and large displacements of order  $v\tau$  occur due to nonequilibrium activity (orange arrows). (b) Best fit values of the active diffusion coefficient, (c) the persistence time and the typical confinement time, (d) the persistence length, and (e) the energy dissipation rate.

agregates, namely about 40 min [35–38].

*Distribution of the vertex displacement.*—To gain further insight into the active component of the dynamics, we compare the PDF of displacement extracted from the simulated trajectories of the vertex dynamics with the experimental distributions [28]. The experimental distribution at short time is Gaussian and entirely controlled by the passive parameters, as confirmed by simulations in the absence of active fluctuations where we use the passive parameters estimated from the fit of the MSD data (see Fig. S6 in [28]). Including the active component of the dynamics leaves us with one remaining free parameter: the average persistence length  $v\tau$  of the large displacements. The short time Gaussian remains unchanged, whereas exponential tails develop at large times in the simulated PDF. The tails are more pronounced as time increases, while the central Gaussian part of the distribution barely changes. We adjust the  $v\tau$  value by matching the tails appearing in the numerical results and the experimental data.

The simulated PDF compares very well with the experiments at large times, showing that our simulations reproduce the evolution of the experimental distributions even beyond the short times [Figs. 2(b-f)]. The order of magnitude of the extracted mean persistence length  $v\tau$  is consistent with our experimental observations [Fig. 3(d)]. We report again the same hierarchy within the Rho pathway, namely an increase of  $v\tau$  from myosin inhibitor to Rho kinase inhibitor, and from Rho kinase inhibitor to Rho in-

hibitor, as a signature of enhanced directed motion. The source of this enhanced motion could be due to actin polymerization, promoted by other signaling pathways, as cdc42 and Rac [39].

*Dissipation.*—The mean rate of energy dissipation is defined as the difference between the power injected by the thermostat and the one that the moving vertex gives back to the surrounding environment via the drag force:  $J = \langle \dot{x}(\gamma\dot{x} - \sqrt{2\gamma k_B T}\xi) \rangle$ , where  $\dot{x}$  is the vertex velocity, and  $\xi$  is a zero-mean Gaussian white noise [10, 11]. It vanishes for systems in a thermodynamic equilibrium state such as steady foams. The active nonequilibrium fluctuations lead to a non zero dissipation rate  $J = kD_A/(1 + \tau k/\gamma)$  [12]. This allows us to predict the amount of energy dissipated by the motor activity in the tissue.

When computing the dissipation rate in the five conditions, it appears as approximately constant except for the depolymerized MT case [Fig. 3(e)]. This suggests that there may be an underlying coupling between mechanical properties of the tissue controlled by the passive parameters  $\{\gamma, k\}$ , and motor activity quantified by  $\{D_A, \tau\}$ . Speculating that the energy provided by the nonequilibrium processes is involved in topological transitions, our result supports that the same amount of energy is dissipated in such events within all the conditions, except in MT depolymerization. In this case, the lower value of  $J$  suggests that a reduced number of topological events occur. This would be consistent with a reduced activity of endocytosis/exocytosis of cadherin, yielding more stable cell-cell interfaces.

*Discussion.*—In this work, we measured the fluctuations of tricellular junctions in epithelial tissues and quantify the nonequilibrium properties of their dynamics. Our analysis is based on a physical modeling which disentangles the active nonequilibrium fluctuations from the thermal equilibrium ones. By fitting the MSD data, we estimated the active diffusion coefficient which characterizes the dynamics at long times and large distances, and we quantified the timescale associated with the nonequilibrium directed motion events. Numerical results demonstrated that our prediction is consistent with the full statistics of the vertices, from which we accessed the typical length of the active large displacements. The extracted parameters reveal that the hierarchy in the pathway controlling the acto-myosin activation is correlated at the mesoscopic level to the vertex fluctuations.

We believe that our work paves the way towards a better understanding of spontaneous topological transformations within tissues. In support of this, we have extracted the MSD from a pair of vertices undergoing a T1 transition, revealing that the transition is correlated to superdiffusive behavior (see Fig. S5 in [28], and movie in [40]). It suggests that active fluctuations, powered by acto-myosin motors and encoded in cell-cell junctions, play a crucial role in the structural rearrangements of tissues.

We thank F. Graner for helpful discussions and a critical

reading of the manuscript. We acknowledge J. W. Nelson for sending the MDCK cell lines. We also thank N. Maggartou for extraction of data and lab members for discussions. This work is supported by CNRS, FRC and University of Strasbourg.

---

\* These authors contributed equally to this work

- [1] F. Jülicher, K. Kruse, J. Prost, and J.-F. Joanny, *Physics Reports* **449**, 3 (2007).
- [2] F. C. MacKintosh and A. J. Levine, *Phys. Rev. Lett.* **100**, 018104 (2008).
- [3] É. Fodor, M. Guo, N. S. Gov, P. Visco, D. A. Weitz, and F. van Wijland, *EPL* **110**, 48005 (2015).
- [4] D. Bi, J. H. Lopez, J. M. Schwarz, and M. L. Manning, *Soft Matter* **10**, 1885 (2014).
- [5] K. Dierkes, A. Sumi, J. Solon, and G. Salbreux, *Phys. Rev. Lett.* **113**, 148102 (2014).
- [6] W. W. Ahmed, É. Fodor, and T. Betz, *BBA - Molecular Cell Research* **1853**, 3083 (2015).
- [7] E. Ben-Isaac, É. Fodor, P. Visco, F. van Wijland, and N. S. Gov, *Phys. Rev. E* **92**, 012716 (2015).
- [8] D. Bi, X. Yang, M. C. Marchetti, and M. L. Manning, ArXiv e-prints (2015), [arXiv:1509.06578](https://arxiv.org/abs/1509.06578).
- [9] W. W. Ahmed, E. Fodor, M. Almonacid, M. Bussonnier, M.-H. Verlhac, N. S. Gov, P. Visco, F. van Wijland, and T. Betz, ArXiv e-prints (2015), [arXiv:1510.08299](https://arxiv.org/abs/1510.08299).
- [10] K. Sekimoto and S. Sasa, *J. Phys. Soc. Jpn.* **66**, 3326 (1997).
- [11] K. Sekimoto, *J. Phys. Soc. Jpn.* **66**, 1234 (1997).
- [12] É. Fodor, K. Kanazawa, H. Hayakawa, P. Visco, and F. van Wijland, *Phys. Rev. E* **90**, 042724 (2014).
- [13] É. Fodor, W. W. Ahmed, M. Almonacid, M. Bussonnier, N. S. Gov, M.-H. Verlhac, T. Betz, P. Visco, and F. van Wijland, ArXiv e-prints (2015), [arXiv:1511.00921](https://arxiv.org/abs/1511.00921).
- [14] R. Farhadifar, J.-C. Roper, B. Aigouy, S. Eaton, and F. Jülicher, *Curr. Bio.* **17**, 2095 (2007).
- [15] J. Käfer, T. Hayashi, A. F. M. Marée, R. W. Carthew, and F. Graner, *Proc. Natl. Acad. Sci. USA* **104**, 18549 (2007).
- [16] M. Rauzi, P. Verant, T. Lecuit, and P.-F. Lenne, *Nat Cell Biol* **10**, 1401 (2008).
- [17] D. Bi, J. H. Lopez, J. M. Schwarz, and M. L. Manning, *Nat. Physics* (2015), [10.1038/nphys3471](https://doi.org/10.1038/nphys3471).
- [18] C. Bertet, L. Sulak, and T. Lecuit, *Nature* **429**, 667 (2004).
- [19] A. C. Martin, M. Kaschube, and E. F. Wieschaus, *Nature* **457**, 495 (2009).
- [20] J. Solon, A. Kaya-Copur, J. Colombelli, and D. Brunner, *Cell* **137**, 1331 (2009).
- [21] C. Guillot and T. Lecuit, *Science* **340**, 1185 (2013).
- [22] M. Rauzi, P.-F. Lenne, and T. Lecuit, *Nature* **468**, 1110 (2010).
- [23] P.-L. Bardet, B. Guirao, C. Paoletti, F. Serman, V. Lopold, F. Bosveld, Y. Goya, V. Mirouse, F. Graner, and Y. Bellaïche, *Developmental Cell* **25**, 534 (2013).
- [24] C. L. Adams, Y. Chen, S. J. Smith, and W. J. Nelson, *J. Cell Biol.* **142**, 1105 (1998).
- [25] A. Doostmohammadi, S. P. Thampi, T. B. Saw, C. T. Lim, B. Ladoux, and J. M. Yeomans, *Soft Matter* **11**, 7328 (2015).
- [26] C. Klingner, A. V. Cherian, J. Fels, P. M. Diesinger, R. Aufschneider, N. Maghelli, T. Keil, G. Beck, I. M. Tolić-Nørrelykke, M. Bathe, and R. Wedlich-Soldner, *J. Cell Biol.* **207**, 107 (2014).
- [27] D. Riveline, E. Zamir, N. Q. Balaban, U. S. Schwarz, T. Ishizaki, S. Narumiya, Z. Kamb, B. Geiger, and A. D. Bershadsky, *J. Cell Biol.* **153**, 1175 (2001).
- [28] See Supplemental Material at [URL will be inserted by publisher] for experimental materials and methods and for details on model, simulations, and data analysis.
- [29] T. Toyota, D. A. Head, C. F. Schmidt, and D. Mizuno, *Soft Matter* **7**, 3234 (2011).
- [30] X. Trepát, M. R. Wasserman, T. E. Angelini, E. Millet, D. A. Weitz, J. P. Butler, and J. J. Fredberg, *Nat. Physics* **5**, 426 (2009).
- [31] P. Bursac, G. Lenormand, B. Fabry, M. Oliver, D. Weitz, V. Viasnoff, J. Butler, and J. J. Fredberg, *Nat. Mater.* **4**, 557 (2005).
- [32] X. Serra-Picamal, V. Conte, R. Vincent, E. Anon, D. T. Tambe, E. Bazellieres, J. P. Butler, J. J. Fredberg, and X. Trepát, *Nat. Physics* **8**, 628 (2012).
- [33] A. Puliafito, L. Hufnagel, P. Neveu, S. Streichan, A. Sigal, D. K. Fygenson, and B. I. Shraiman, *Proc. Natl. Acad. Sci. USA* **109**, 739 (2012).
- [34] S. Stehbens and T. Wittmann, *J. Cell Biol.* **198**, 481 (2012).
- [35] G. Forgacs, R. A. Foty, Y. Shafir, and M. S. Steinberg, *Biophys J* **74**, 2227 (1998).
- [36] K. Guevorkian, M.-J. Colbert, M. Durth, S. Dufour, and F. Brochard-Wyart, *Phys. Rev. Lett.* **104**, 218101 (2010).
- [37] P. Marmottant, A. Mgharbel, J. Käfer, B. Audren, J.-P. Rieu, J.-C. Vial, B. van der Sanden, A. F. M. Marée, F. Graner, and H. Delanoë-Ayari, *Proc. Natl. Acad. Sci. USA* **106**, 17271 (2009).
- [38] T. V. Stirbat, A. Mgharbel, S. Bodennec, K. Ferri, H. C. Mertani, J.-P. Rieu, and H. Delanoë-Ayari, *PLoS ONE* **8**, e52554 (2013).
- [39] S. Etienne-Manneville and A. Hall, *Nature* **420**, 629 (2002).
- [40] See Supplemental Material at [URL will be inserted by publisher] for a movie of a typical T1 transition. Scale bar is 10  $\mu\text{m}$ , time is in hh:mm; red and blue points record vertex trajectories.